

This is the preprint of the following article:

Hubman A, Merzel F. Determination of thermal conductivities in liquids by identifying heat transport in nonequilibrium MD simulations. *Journal of Molecular Liquids*. 2023; (370): 1–7.

doi: 10.1016/j.molliq.2022.120916

which has been published in final form at:

<http://dx.doi.org/10.1016/j.molliq.2022.120916>

Determination of thermal conductivities in liquids by identifying heat transport in nonequilibrium MD simulations

Anže Hubman^{a,b}, Franci Merzel^{a,*}

^aLaboratory for Molecular Structural Dynamics, Theory Department, National Institute of Chemistry, Hajdrihova 19, 1000 Ljubljana, Slovenia

^bFaculty of Chemistry and Chemical Technology, University of Ljubljana, Večna pot 113, 1000 Ljubljana, Slovenia

Abstract

A new method for efficient and robust determination of thermal conductivity in liquids is presented. The method is based on the search for an optimal agreement between the analytical solution of the heat transfer in a continuum model described by Fourier law and the relaxation of thermal inhomogeneity simulated by nonequilibrium MD simulations. Our approach exploits a transient regime in which a system relaxes towards equilibrium after the introduction of a small temperature perturbation in a spatially confined part of the system. The applicability of this new method is demonstrated on liquid argon and two water models, the mW and SPC models.

Keywords: MD simulations, heat transfer, thermal conductivity

1. Introduction

Thermal conductivity (κ) is one of the fundamental material properties and measures the rate at which thermal equilibrium is established. In the past, a substantial effort has been devoted to the development of computational methods which allow one to determine thermal conductivities of liquids, crystals, and glasses by exploiting molecular dynamics (MD) simulations [1]. Accurate and reliable *in silico* methods are especially important in cases where an experimental determination of transport coefficients is challenging as for

*Corresponding author

Email address: franci.merzel@ki.si (Franci Merzel)

example in ionic melts [2, 3] or liquids under extreme pT conditions [4, 5]. Ionic melts and specifically understanding of their thermal properties are now becoming increasingly more important due to their use as heat-transfer fluids in solar power plants [6] and molten salt nuclear reactors [7]. State of the art computational methods for the determination of thermal conductivities (and other transport coefficients as well) generally fall into one of the two categories: equilibrium and non-equilibrium methods.

Equilibrium methods are rooted in the Green-Kubo (GK) theory of linear response [8, 9] where one is required to evaluate the integral of the heat flux autocorrelation function which, for three-dimensional isotropic case, reads as:

$$\kappa = \frac{1}{3k_bVT^2} \int_0^{t_0 \rightarrow \infty} \langle \mathbf{J}(0) \cdot \mathbf{J}(\tau) \rangle d\tau. \quad (1)$$

Here V and T are the volume and the temperature of a system, respectively, and $\langle \rangle$ stands for the ensemble average. Despite the theoretical elegance, the GK method is associated with practical limits raised by the slow convergence of κ with the available simulation time t_0 . In case of slow relaxation in the system, long-time tails are present in the autocorrelation function. Moreover, the autocorrelation function becomes dominated by statistical noise at large τ values which implies that the upper integration limit t_0 significantly affects the result [10, 11, 12]. Therefore, large simulation cells and long trajectories are usually required to obtain well-converged results. The aforementioned problems were significantly overcome very recently by the introduction of the *cepstral analysis* which allows relatively accurate estimation of transport coefficients even from trajectories affordable by *ab-initio* MD simulations [13, 14]. Another recently introduced equilibrium approach by Cheng & Frenkel is based on the computation of the thermal conductivity solely from an analysis of particle density fluctuations [15] and therefore bypasses the computation of the heat flux.

In order to overcome the difficulties of the equilibrium methods described above, several nonequilibrium (NEMD) methods have been developed which rely on continuum description

of heat conduction given by Fourier law:

$$\mathbf{J} = -\kappa \nabla T. \quad (2)$$

A common trait of most NEMD methods is the direct use of the Fourier law. For that purpose, one either imposes a temperature gradient along one direction of a simulation cell and measures the generated heat flux [16] (direct-NEMD) or one imposes the heat flux and measures the established temperature gradient [17] (reverse-NEMD). In both cases κ is estimated as a slope of J_x versus dT/dx (x is the direction along the temperature gradient) after a non-equilibrium steady state has been reached. These methods require shorter simulation times but may suffer from convection problems and significant size effects. In the context of NEMD methods, it is much less common to deviate from the non-equilibrium steady state as explained above and use a transient regime instead where a relaxation of temperature perturbation is monitored. Such ideas were mostly applied to studies of heat conduction in crystalline and amorphous solids in the context of phonons [18, 19, 20] and transient melting at the nanoscale [21].

Here we present a new non-equilibrium scheme for the determination of thermal conductivity of liquids based on continuum description of heat transfer. The method exploits the transient regime where a system undergoes a thermal relaxation towards equilibrium after the introduction of a small temperature perturbation. Our approach is simple to implement, easy to run in parallel and is compatible with periodic boundary conditions (PBCs) commonly applied in bulk MD simulations.

2. Model

Let us consider a bulk liquid in a form of extended linear filament with a temperature inhomogeneity present along the main axis. Heat transfer in such a system is described by combining the Fourier law and continuity equation which leads to the heat transport equation

$$\frac{\partial T(x, t)}{\partial t} = \frac{\kappa}{\rho c_p} \frac{\partial^2 T(x, t)}{\partial x^2}, \quad (3)$$

with ρ standing for the density and c_p for specific heat. Assuming the fixed form of initial temperature profile $T_0(x, t = 0)$ we can obtain temperature profile at any time $t > 0$ by the general solution of eq. (3):

$$T(x, t) = \frac{1}{2a\sqrt{\pi t}} \int_{-\infty}^{\infty} T_0(x') \exp\left(-\frac{(x-x')^2}{4a^2t}\right) dx', \quad (4)$$

where we introduce the parameter $a = \sqrt{\kappa/(\rho c_p)}$.

Although the equation (4) generally describes heat conduction in macroscopic continuum medium, we assume that it also can correctly describe heat conduction for sufficiently large microscopic systems, *i.e.* sufficiently dense systems containing large enough number of atoms, $\mathcal{N} > \mathcal{N}_c$, above some threshold value \mathcal{N}_c . If microscopic system is supposed to obey the Fourier law, then for a properly set parameter a the solution (4) should match the temperature profile derived from the simulated particle velocity distributions at the same time $t > t_0$ given that the analytical and simulated temperature profiles at the time t_0 are equal. Furthermore, if matching between analytical and simulated temperature profiles is found to exist for a given value of a at any instant of time during the relaxation and persists over the size range $\mathcal{N} > \mathcal{N}_c$, then the fitting parameter a can be used to determine the thermal conductivity κ of the simulated system. Standard MD simulations of bulk media imply periodic boundary conditions (PBC), which means that any inhomogeneity in the primary simulation cell representing the finite volume of the system is necessarily replicated in all surrounding image cells. Thus, in order to make the analogy of the temperature profile $T(x)$ in the simulated system under PBC and its continuum counterpart, we should also apply the periodic condition, $T(x \pm L) = T(x)$, in the analytical model with L being the length of the primary cell. The analytical solution for the time dependent temperature profile within the range of the primary cell, $[-L/2, L/2]$, which is explicitly derived in Appendix A, consists of contributions from the neighboring image cells,

$$T(x, t) = \frac{1}{2a\sqrt{\pi t}} \sum_{n=-N}^{n=N} \exp\left(-\frac{(nL)^2}{4a^2t}\right) \int_{-L/2}^{L/2} T_0(x') \exp\left(-\frac{(x-x')^2 - 2nL(x-x')}{4a^2t}\right) dx', \quad (5)$$

where n indexes neighboring images as indicated in Figure 1.

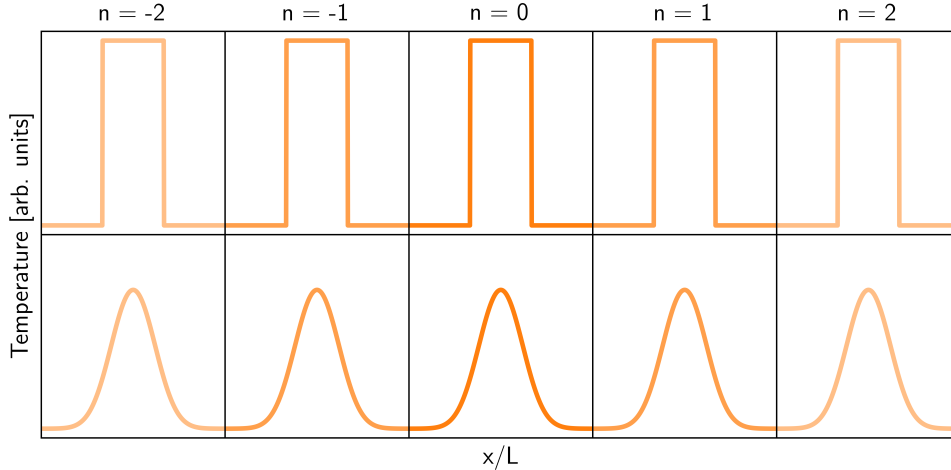


Figure 1: A schematic representation of temperature profiles in continuum linear filament applying PBC along x -axis. Upper and lower rows display the profile $T_0(x)$ at the beginning, and at some later time t , $T(x, t)$, respectively. The central cell ($n = 0$) corresponds to the primary cell.

Derivation of the thermal conductivity can be thus based on fitting of the analytical solution of eq. (5) to temperature profiles collected from MD simulations at different evolution times from some well defined initial temperature profile.

In what follows the above approach will be validated on three carefully chosen systems: liquid argon, Stillinger-Weber monoatomic water model (mW) [22] and the SPC [23] water model.

3. Simulation setup

All MD simulations were performed using LAMMPS [24] combined with several in-house developed computer codes for the purposes of thermostatting and post-processing. A standard velocity-Verlet integration scheme was used and the periodic boundary conditions were imposed in all directions.

Pairwise interactions in liquid argon, a paradigmatic example of a simple liquid, were

described using the Lennard-Jones potential:

$$U(r) = 4\epsilon \left[\left(\frac{\sigma}{r} \right)^{12} - \left(\frac{\sigma}{r} \right)^6 \right] \quad (6)$$

and truncated at $r_c = 2.5\sigma$. Unless stated otherwise, simulations were performed with 6.000 atoms. For the sake of comparison with a previous study by Ercole et. al. [13] we ran our calculations at the density $\rho = 1.55 \text{ g/cm}^3$ and $T_0 = 220 \text{ K}$, adopting $\epsilon/k_B = 119.8 \text{ K}$ and $\sigma = 0.3405 \text{ nm}$ [25]. Equations of motion were integrated using a timestep of 4 fs. For monoatomic water (mW) introduced by Molinero and Moore we used the Stillinger-Weber force-field which also contains many-body interactions. As discussed by other authors before, the standard expression for heat flux should not be used in the case of many-body potentials [26]. Thermal conduction in mW water has been studied by Cheng and Frenkel who used the recently introduced WAVE method. We performed our simulations with 9.000 atoms adopting the same thermodynamic conditions as in [15] ($T = 800 \text{ K}$ and $p = 35.6 \text{ atm}$) and a timestep of 4 fs.

Lastly we check the performance of our method on bulk water represented by SPC water model. We used 3000 molecules and ran the simulations at $\rho = 1.0 \text{ g/cm}^3$ and $T = 300 \text{ K}$ with a timestep of 1 fs. Bond lengths and HOH angles were constrained using SHAKE [27]. Long-range interactions were taken into account by means of PPPM [28] method with a force accuracy of 10^{-5} .

The workflow of our approach is as follows. First, a cubic simulation box with an edge L is created and the atoms are placed at random positions. The system is extensively equilibrated at T_0 in the NVT ensemble using Nose-Hoover thermostat [29, 30]. After the initial equilibration, the system is divided into N_s slices along the x direction (see Fig. 2) and the Nose-Hoover thermostat is switched off. To create a temperature perturbation, the atomic velocities in each slice are rescaled by a factor

$$\lambda = \sqrt{\frac{T'}{T_0}}, \quad (7)$$

where T' is given by the shape of the perturbation that we want to impose. For SPC water, all atoms in a molecule are rescaled by the same factor. Here we have used a perturbation in the form of a boxcar function:

$$T'(x, t = 0) = \begin{cases} T_0 + \Delta T & ; \frac{L-d}{2} \leq x \leq \frac{L+d}{2} \\ T_0 & \text{otherwise} \end{cases}$$

where $0 \leq x \leq L$. Such rescaling procedure is applied for 500 ps every $\Delta t = 20$ fs. After each rescaling event, atom velocities are corrected by the amount of the center of mass velocity of entire system to assure zero total momentum. Between two rescaling events, the system is allowed to evolve microcanonically. After a non-equilibrium steady state has been reached, we keep the same protocol for as long as required to extract M frames which serve as a starting point for relaxation. Usually, $M = 1000$ is sufficient to obtain well-converged results. The aforementioned frames are extracted every $\tau = 800$ fs which is enough to ensure that two successive starting configurations are statistically independent of each other. The value of τ can be conveniently estimated for instance from velocity autocorrelation function. Lastly, M independent microcanonical (NVE) simulations are performed and the atomic *velocities* are stored in each slice. The length of each NVE run is typically between 10-20 ps which is sufficient for the system to almost completely relax to equilibrium. Obviously, the length of NVE runs has to be adjusted according to the magnitude of L , since for larger simulation boxes the relaxation proceeds slower and vice versa. The final temperature in j -th slice at time t is obtained from:

$$T_j(t) = \frac{1}{k_B} \left\langle \frac{1}{N_{DOF}} \sum_{i=1}^N m_i v_i^2 \right\rangle. \quad (8)$$

Here T_j is computed from velocities of atoms which, at time t , belong to the j -th slice and the constrained degrees of freedom in case of SPC water model are carefully omitted in N_{DOF} . Note that the velocities stored in each slice are taken from all M NVE runs and a single calculation of a temperature per slice is made.

In order to obtain thermal conductivity κ from thermal diffusivity α , the density and the isobaric heat capacity c_p are required ($\alpha = \kappa/\rho c_p$). Given that all simulations are performed at constant volume, the density is readily available and the heat capacity can be routinely evaluated from a slope of enthalpy $H(T)$ versus temperature T in the interval from T_0 to $T_0 + \Delta T$ using a separate set of NpT simulations.

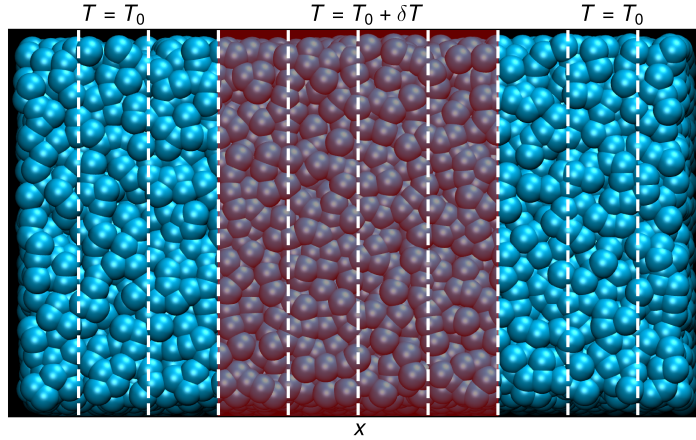


Figure 2: The simulation box divided into N_s slices. Figure was generated using VMD [\[31\]](#) and `matplotlib`.

4. Results and Discussion

In the following, we test our approach on liquid argon in a superfluidic state, mW and SPC water models as described in Simulation setup (Section 3) and summarized in the Appendix B. We begin with a short description of time series analysis ($\kappa(t)$) through which the final conductivity along with the error can be estimated. We continue with the evaluation of the robustness of our method to the choice of several parameters: the number of neighboring periodic images required, the width of the perturbation and the magnitude of ΔT . We finish our discussion by examining size effects for Lennard-Jones fluid and give a brief overview of results for mW and SPC water. The number of slices is fixed at $N_s = 30$.

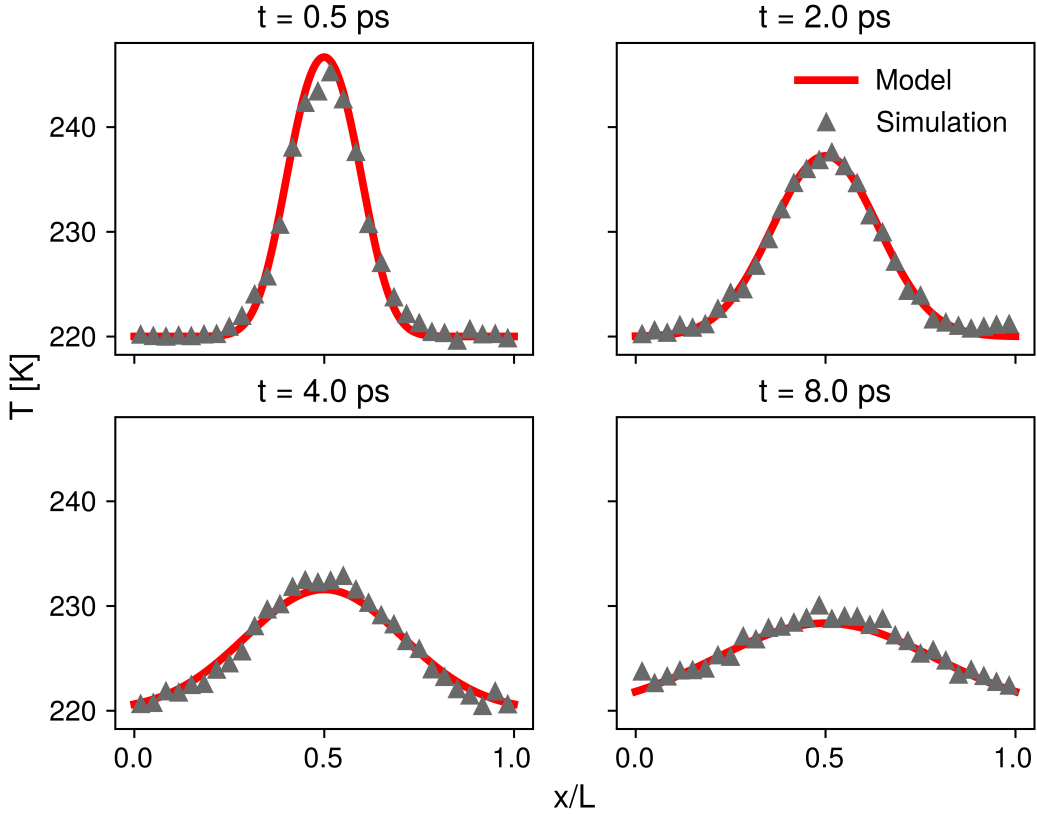


Figure 3: Snapshots of temperature profiles during relaxation at various times for liquid argon.

4.1. Liquid argon

Using the simulation protocol described in Section 3, we obtain temperature profiles $T(x, t)$ (see Figure 3) which are used to compute the thermal conductivity by fitting them with the analytical solution given by Eq. (5). We perform a separate fit at each t and thus obtain a time series $\kappa(t)$ from which the final conductivity along with the error estimate is extracted.

4.1.1. Time series analysis

A typical shape of $\kappa(t)$ is shown in Figure 4. For $t < 2$ ps, κ shows significant instability which we suspect is due to the memory effect of a thermostat. Nonetheless, for $t > 2$ ps, κ quickly stabilizes and generally begins to oscillate around the correct value of thermal conductivity. Therefore values of κ for $t < 2$ ps are discarded from further discussion. The shape

of $\kappa(t)$ for $t > 2$ ps shows regular oscillations which are not merely statistical fluctuations. Given that simulations are performed under periodic boundary conditions, such oscillations are expected. As the temperature perturbation relaxes, the thermal wave collides with the ones from its neighboring images. When the thermal wave bounces back, κ is underestimated and vice versa as the wave relaxes again. Thermal waves are not predicted by Fourier law or heat equation which is the basis of our model. We did not try to incorporate their presence in our analytical solution but rather account for them in the posteriori analysis. A thorough discussion on thermal waves and non-Fourier types of heat conduction can be found for instance in Ref. [32]. As far as our method is concerned, for smaller simulation boxes and sufficient averaging over a large number of trajectories it is possible to nearly eliminate the presence of a wave in the final $\kappa(t)$. Conversely, for larger simulation boxes the wave persists which is expected given that the creation of a coherent wave is more likely (compare for instance Figure 4 and Figure 5a). In Figure 4 we show that if running average over a well-converged $\kappa(t)$ is performed, the presence of thermal waves is not problematic to obtain the correct value of thermal conductivity since running average is a well-behaved function. More specifically, for a set of N equally spaced temperature profiles from a trajectory of length $t_{max} = N\Delta t$, we define the running average over $\kappa(t)$ as:

$$\bar{\kappa}(t) = \frac{1}{j - k + 1} \sum_{i=k}^j \kappa_i. \quad (9)$$

Here k corresponds to the moment in time t_0 from which averaging takes place, namely $t_0 = k\Delta t$, $t = j\Delta t$ (for $t = t_{max}$, $j = N$), and $1/\Delta t$ is the sampling frequency.

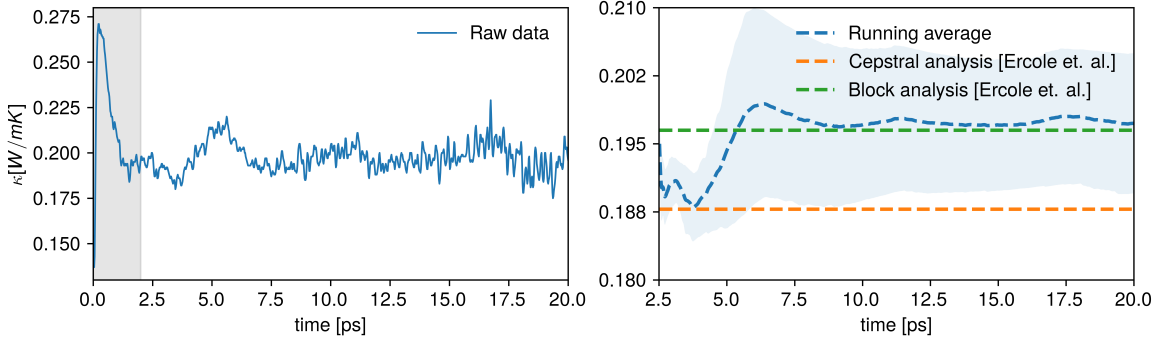


Figure 4: Raw data (left) and running average (right) of thermal conductivity shown for a system of liquid argon where $\Delta T = 30$ K, $d/L = 0.2$ and $N_s = 30$. Two neighboring images ($n = 2$) were included in the fitting procedure. Our estimation of κ agrees well with values obtained by Ercole et. al. [13] within the statistical error.

To summarize, if well-converged κ is to be obtained from a stable running average over $\kappa(t)$, it should not matter whether oscillations are present in the simulation when solely trying to extract thermal conductivity; they contribute only to the larger standard deviation.

Another important parameter which influences the rate of convergence of $\kappa(t)$ with respect to the number of required simulated trajectories is τ as defined in *Simulation setup*. An optimal choice of τ can be estimated from a velocity autocorrelation function (VACF). The suggested choice of τ is the moment at which VACF reaches 0, which ensures that two successive starting configurations, used to study an independent thermal relaxation, are indeed uncorrelated.

4.1.2. Neighboring periodic images corrections

As shown in Section 2, the correct treatment of heat transfer for the setup considered here includes taking into account the periodic boundary conditions. Here we identify the minimum number of neighboring periodic replicas of the central box ($n = 0$) that are necessary to ensure that the relaxation of a temperature perturbation is correctly described for the whole duration of our simulations (i.e. until thermal equilibrium is nearly established again). We also compare our predictions with the model which ignores the periodicity and assumes that the perturbation is allowed to spread to infinite media on both sides of the central box. The solution of the heat equation for the latter case can be evaluated analytically and has a

well-known form given by:

$$T(x, t) = T_0 + \frac{1}{2}\Delta T \left[\operatorname{erf} \left(\frac{\frac{1}{2}(L+d) - x}{\sqrt{4\alpha t}} \right) - \operatorname{erf} \left(\frac{\frac{1}{2}(L-d) - x}{\sqrt{4\alpha t}} \right) \right]. \quad (10)$$

As expected, for short t ($t < 7$ ps) it is not important whether the system is treated as periodic or infinite on both sides of the central box. The latter approximation, however, quickly breaks down as demonstrated in Figure 5 (left). To achieve well converged $\kappa(t)$ throughout the whole relaxation process under periodic geometry, it is necessary to include neighboring image corrections up to at least $n = 2$. Nonetheless, it is actually not necessary to sample the whole relaxation to achieve well converged κ since running average over $\kappa(t)$ stabilizes much faster (see Figure 4). Therefore as shown in Figure 5 corrections up to $n = 1$ are already sufficient. Throughout this work, we have consistently used corrections up to $n = 2$.

4.1.3. Width of a perturbation and the magnitude of ΔT

To check how the shape of a perturbation affects the estimation of thermal conductivity, we performed simulations for various widths (d) of the slab in which a thermal perturbation is introduced, and magnitudes of ΔT by keeping the number of slices and the system size fixed ($N_s = 30, N = 6000$). Simulation parameters that were used and corresponding results are given in Table 1.

| d/L | ΔT [K] | κ [W/mK] |
|-------|----------------|--------------------|
| 1/5 | 30 | 0.1969 ± 0.007 |
| 2/5 | 30 | 0.1927 ± 0.007 |
| 1/5 | 50 | 0.1958 ± 0.005 |

Table 1: Values of κ for various values of d/L and ΔT .

We conclude that neither the magnitude of ΔT nor the width of a perturbation do not significantly affect κ since all values listed in Table 1 coincide within the statistical error, indicating the robustness of our method. Note that the higher values of ΔT may speed up the convergence of temperature profiles and therefore the convergence of κ itself since

the signal to noise ratio is increased. However, too high values of ΔT can cause significant changes in both κ and c_p . Therefore, we suggest using modest values of ΔT up to 20% of the reference temperature.

4.1.4. Size effects

We finish our discussion by examining the influence of L (and the number of atoms N) on predicted values of κ . Our systems are cubic and therefore all cell parameters are changed simultaneously ($L = L_x = L_y = L_z$). The relationship between systems size and the number of atoms is given in the Table 2.

As discussed by several authors before, thermal conductivity predicted by NEMD methods is generally underestimated for small L . This effect is severe for solid systems when the phonon mean free path is smaller than L [19]. For liquid systems, size effects also exist and it has been suggested, for example, that $\kappa \propto 1/\sqrt{L_x}$ for a Lennard-Jones fluid when the cross section is kept constant and the simulation cell is elongated along x -axis [33].

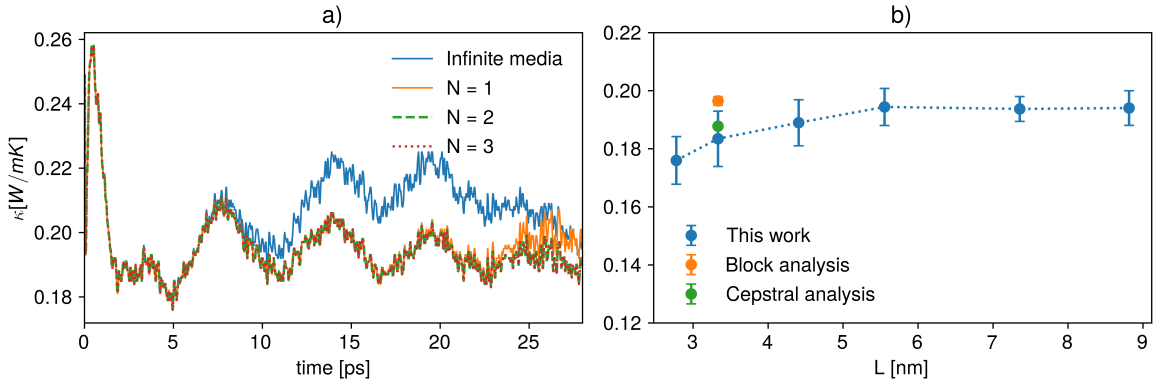


Figure 5: Dependence of $\kappa(t)$ with respect to the maximum range N of neighboring images included in the analytical solution (5), which was used in the fitting procedure (left) and size dependence of $\kappa(L)$ as predicted by our method (right).

| L [Å] | \mathcal{N} |
|---------|---------------|
| 27.76 | 500 |
| 33.70 | 894 |
| 44.07 | 2000 |
| 55.53 | 4000 |
| 75.36 | 10000 |
| 88.14 | 16000 |

Table 2: Number of atoms \mathcal{N} in the various simulation cells of size L .

Here we do not wish to discuss the scaling relationship $\kappa(L)$ as predicted by our method in detail, but merely provide guidance for selecting the optimal L . Figure 6 clearly shows that κ is underestimated for small L in agreement with studies mentioned before. Thermal conductivity converges near $L \approx 4.4$ nm which, for the density used here, corresponds to $\mathcal{N} \approx 2000$ atoms. All values of κ beyond this threshold agree within statistical uncertainty. Nonetheless, this threshold may depend on the density and therefore an analysis of size effects is highly suggested to obtain reliable and well-converged thermal conductivity.

4.2. Monoatomic water model

Monoatomic water (mW) model is a simple example of a liquid which contains many-body interactions. As such (and as briefly mentioned before) the textbook definition of heat fluxes based on pairwise interactions is not applicable in this case and the correct definition of heat fluxes is non-trivial. In our method an explicit definition of heat fluxes is not needed thus making our approach much more elegant. Simulations performed here to illustrate the applicability of our approach were run at $T_0 = 800$ K which is also a range of thermodynamic conditions relevant for e.g. industrially important ionic melts. Therefore we expect similar performance for ionic systems. Cheng and Frenkel determined the thermal conductivity of mW using WAVE method. They determined $\kappa = 0.16$ W/mK (6,912 atoms) and $\kappa = 0.17$ W/mK (27,648 atoms), respectively. Our method predicts $\kappa = 0.1721$ W/mK in good agreement with predictions from WAVE. Our approach therefore also performs well even at fairly extreme conditions.

4.3. SPC water model

Lastly we devote our attention to a simple molecular fluid - an SPC water model. Heat transport in molecular fluids is significantly more difficult to simulate due to additional degrees of freedom with the most problematic ones being the bond vibrations and angle bendings. In the results presented here the bonds and angles have been constrained using the SHAKE algorithm which effectively means that the degrees of freedom which may act as energy sinks are eliminated. Indeed with constraints we reach excellent agreement between our method ($\kappa = 0.768$ W/mK) and the previous works where the authors have used either the Green-Kubo [34] ($\kappa = 0.776$ W/mK) or the Müller-Plathe [34] ($\kappa = 0.802$ W/mK) approach. If the constraints are released, our method fails to correctly simulate heat conduction since the kinetic energy is drained into the vibrational modes. We expect our approach will perform similarly with other liquids be it in flexible or rigid flavors.

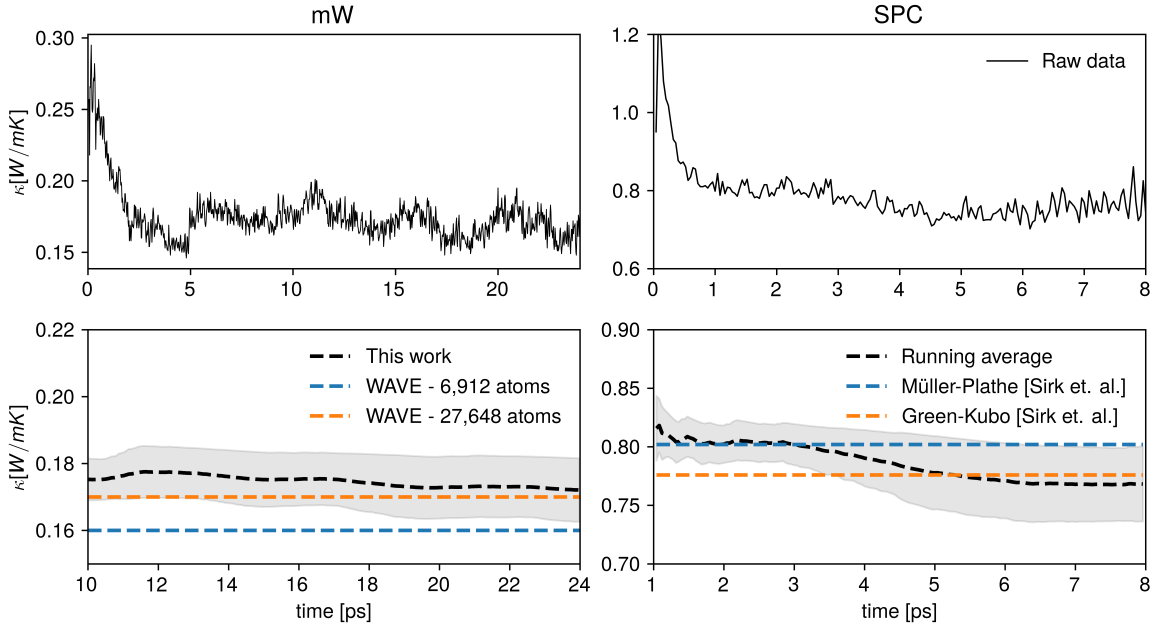


Figure 6: Time series analysis for mW (left) and SPC water (right).

5. Conclusions

In the present work, we have successfully demonstrated and thoroughly evaluated our approach to calculating thermal conductivities in atomistic and molecular liquids using nonequilibrium molecular dynamics. The method presented here is simple, robust, effective, and can be easily performed in parallel. It is independent of the choice of the interatomic potentials and can be applied to both pairwise and many-body potentials. An important advantage is that our approach does not require an a priori definition of the heat fluxes, which is known to be problematic in cases where fluids cannot be described by a pairwise interatomic potential. The efficiency of the method is evidenced by the proper treatment of periodic boundary conditions in the derivation of the analytical solution in reference continuum models.

6. Acknowledgements

We gratefully acknowledge funding by the Slovenian Research Agency (ARRS) through the research Grant no. P1-0010.

References

- [1] P. Ungerer, C. Nieto-Draghi, B. Rousseau, G. Ahunbay, V. Lachet, Molecular simulation of the thermophysical properties of fluids: From understanding toward quantitative predictions, *J. Mol. Liq.* 134 (2007) 71–89. [doi:10.1016/j.molliq.2006.12.019](https://doi.org/10.1016/j.molliq.2006.12.019).
- [2] M. Salanne, C. Simon, P. Turq, P. A. Madden, Heat-transport properties of molten fluorides: Determination from first-principles, *Journal of Fluorine Chemistry* 130 (2009) 38–44. [doi:10.1016/j.jfluchem.2008.07.013](https://doi.org/10.1016/j.jfluchem.2008.07.013).
- [3] N. Ohtori, M. Salanne, P. A. Madden, Calculations of the thermal conductivities of ionic materials by simulation with polarizable interaction potentials, *J. Chem. Phys.* 130 (2009) 104507. [doi:10.1063/1.3086856](https://doi.org/10.1063/1.3086856).

- [4] M. Pozzo, C. Davies, D. Gubbins, D. Alfe, Thermal and electrical conductivity of iron at earth's core conditions, *Nature* 485 (2021) 355. [doi:10.1038/nature11031](https://doi.org/10.1038/nature11031).
- [5] F. Grasselli, L. Stixrude, S. Baroni, Heat and charge transport in h2o at ice-giant conditions from ab initio molecular dynamics simulations, *Nature Communications* 11 (2020) 3605. [doi:10.1038/s41467-020-17275-5](https://doi.org/10.1038/s41467-020-17275-5).
- [6] K. Vignarooban, X. H. Xu, A. Arvay, K. Hsu, A. M. Kannan, Heat transfer fluids for concentrating solar power systems - a review, *Applied Energy* 146 (2015) 383–396. [doi:10.1016/j.apenergy.2015.01.125](https://doi.org/10.1016/j.apenergy.2015.01.125).
- [7] R. R. Romatoski, L. W. Hu, Fluoride salt coolant properties for nuclear reactor applications: A review, *Annals of Nuclear Energy* 109 (2017) 635–647. [doi:10.1016/j.anucene.2017.05.036](https://doi.org/10.1016/j.anucene.2017.05.036).
- [8] M. Green, Markoff random processes and the statistical mechanics of time-dependent phenomena. ii. irreversible processes in fluids, *Journal of Chemical Physics* 22 (1954) 398. [doi:10.1063/1.1740082](https://doi.org/10.1063/1.1740082).
- [9] R. Kubo, Statistical-mechanical theory of irreversible processes. i. general theory and simple applications to magnetic and conduction problems, *Journal of the Physical Society of Japan* 12 (1957) 570–586. [doi:10.1143/JPSJ.12.570](https://doi.org/10.1143/JPSJ.12.570).
- [10] Y. Zhang, A. Otani, E. J. Maginn, Reliable viscosity calculation from equilibrium molecular dynamics simulations: A time decomposition method, *Journal of Chemical Theory and Computation* 11 (2015) 3537–3546. [doi:10.1021/acs.jctc.5b00351](https://doi.org/10.1021/acs.jctc.5b00351).
- [11] L. S. Oliveira, P. A. Greaney, Method to manage integration error in the green-kubo method, *Physical Review E* 95 (2017) 023308. [doi:10.1103/PhysRevE.95.023308](https://doi.org/10.1103/PhysRevE.95.023308).
- [12] J. Chen, G. Zhang, How to improve the accuracy of equilibrium molecular dynamics for computation of thermal conductivity?, *Physics Letters A* 374 (2010) 2392–2396. [doi:10.1016/j.physleta.2010.03.067](https://doi.org/10.1016/j.physleta.2010.03.067).

- [13] L. Ercole, A. Marcolongo, S. Baroni, Accurate thermal conductivities from optimally short molecular dynamics simulations, *Scientific Reports* 7 (2017) 15835. [doi:10.1038/s41598-017-15843-2](https://doi.org/10.1038/s41598-017-15843-2).
- [14] R. Bertossa, F. Grasselli, L. Ercole, S. Baroni, Theory and numerical simulation of heat transport in multicomponent systems, *Physical Review Letters* 122 (2019) 255901. [doi:10.1103/PhysRevLett.122.255901](https://doi.org/10.1103/PhysRevLett.122.255901).
- [15] B. Cheng, D. Frenkel, Computing the heat conductivity of fluids from density fluctuations, *Physical Review Letters* 125 (2020) 130602. [doi:10.1103/PhysRevLett.125.130602](https://doi.org/10.1103/PhysRevLett.125.130602).
- [16] T. Ikeshoji, B. Hafskjold, Nonequilibrium molecular-dynamics calculation of heat-conduction in liquid and through liquid-gas interface, *Molecular Physics* 81 (1994) 251–261. [doi:10.1080/00268979400100171](https://doi.org/10.1080/00268979400100171).
- [17] F. Müller-Plathe, A simple nonequilibrium molecular dynamics method for calculating the thermal conductivity, *Journal of Chemical Physics* 106 (1997) 6082–6085. [doi:10.1063/1.473271](https://doi.org/10.1063/1.473271).
- [18] E. Lampin, P. L. Palla, P. A. Francioso, F. Cleri, Thermal conductivity from approach-to-equilibrium molecular dynamics, *Journal of Applied Physics* 114 (2013) 033525. [doi:10.1063/1.4815945](https://doi.org/10.1063/1.4815945).
- [19] C. Melis, R. Dettori, S. Vandermeulen, L. Colombo, Calculating thermal conductivity in a transient conduction regime: theory and implementation, *European Physical Journal B* 87 (2014) 96. [doi:10.1140/epjb/e2014-50119-0](https://doi.org/10.1140/epjb/e2014-50119-0).
- [20] R. J. Hulse, R. L. Rowley, N. V. Wilding, Transient nonequilibrium molecular dynamic simulations of thermal conductivity: 1. simple fluids, *International Journal of Thermophysics* 26 (2005) 1–12. [doi:10.1007/s10765-005-2349-z](https://doi.org/10.1007/s10765-005-2349-z).

- [21] F. Font, F. Bresme, Transient melting at the nanoscale: A continuum heat transfer and nonequilibrium molecular dynamics approach, *Journal of Physical Chemistry C* 122 (2018) 17481–17489. [doi:10.1021/acs.jpcc.8b02367](https://doi.org/10.1021/acs.jpcc.8b02367).
- [22] V. Molinero, E. B. Moore, Water modeled as an intermediate element between carbon and silicon, *Journal of Physical Chemistry B* 113 (2009) 4008–4016. [doi:10.1021/jp805227c](https://doi.org/10.1021/jp805227c).
- [23] H. J. C. Berendsen, J. R. Grigera, T. P. Straatsma, The missing term in effective pair potentials, *Journal of Physical Chemistry* 91 (1987) 6269–6271. [doi:10.1021/j100308a038](https://doi.org/10.1021/j100308a038).
- [24] S. Plimpton, Fast parallel algorithms for short-range molecular-dynamics, *Journal of Computational Physics* 117 (1995) 1–19. [doi:10.1006/jcph.1995.1039](https://doi.org/10.1006/jcph.1995.1039).
- [25] L. A. Rowley, D. Nicholson, N. G. Parsonage, Monte-carlo grand canonical ensemble calculation in a gas-liquid transition region for 12-6 argon, *Journal of Computational Physics* 17 (1975) 401–414. [doi:10.1016/0021-9991\(75\)90042-X](https://doi.org/10.1016/0021-9991(75)90042-X).
- [26] P. Boone, H. Babaei, C. E. Wilmer, Heat flux for many-body interactions: Corrections to lammps, *Journal of Chemical Theory and Computation* 15 (2019) 5579–5587. [doi:10.1021/acs.jctc.9b00252](https://doi.org/10.1021/acs.jctc.9b00252).
- [27] J. P. Ryckaert, G. Ciccotti, H. J. C. Berendsen, Numerical-integration of cartesian equations of motions of a system with constraints-molecular-dynamics of n-alkanes, *Journal of Computational Physics* 23 (1977) 327–341. [doi:10.1016/0021-9991\(77\)90098-5](https://doi.org/10.1016/0021-9991(77)90098-5).
- [28] R. W. Hockney, J. W. Eastwood, *Computer simulation using particles*, CRC Press, New York, 1988.
- [29] S. Nose, A unified formulation of the constant temperature molecular-dynamics methods, *Journal of Chemical Physics* 81 (1984) 511–519.

- [30] W. G. Hoover, Canonical dynamics-equilibrium phase-space distributions, *Physical Review A* 31 (1985) 1695–1697. [doi:10.1063/1.447334](https://doi.org/10.1063/1.447334).
- [31] W. Humphrey, A. Dalke, K. Schulten, Vmd:visual molecular dynamics, *Journal of Molecular Graphics and Modelling* 14 (1996) 33–38. [doi:10.1016/0263-7855\(96\)00018-5](https://doi.org/10.1016/0263-7855(96)00018-5).
- [32] A. H. Akbarzadeh, Y. Cui, Z. T. Chen, Thermal wave: from nonlocal continuum to molecular dynamics, *RSC Advances* 7 (2017) 13623–13636. [doi:10.1039/C6RA28831F](https://doi.org/10.1039/C6RA28831F).
- [33] F. Ogushi, S. Yukawa, Heat conduction of lennard-jones particle system in supercritical fluid phase, *Journal of the Physical Society of Japan* 74 (2005) 827–830. [doi:10.1143/JPSJ.74.827](https://doi.org/10.1143/JPSJ.74.827).
- [34] T. W. Sirk, S. Moore, E. F. Brown, Characteristics of thermal conductivity in classical water models, *Journal of Chemical Physics* 138 (2013) 064505. [doi:10.1063/1.4789961](https://doi.org/10.1063/1.4789961).

7. Appendix

A Derivation of equation (5)

Suppose $T_0(x)$ is periodic function with periodicity L corresponding to the initial temperature profile along linear filament as shown in Figure 1. The analytical solution for the time dependent temperature profile for $x \in [-l/2, l/2]$ according to (4) is given by the sum from individual intervals:

$$\begin{aligned}
 T(x, t) &= \frac{1}{2a\sqrt{\pi t}} \int_{-\infty}^{\infty} T_0(x') \exp\left(-\frac{(x-x')^2}{4a^2t}\right) dx' = \\
 &= \frac{1}{2a\sqrt{\pi t}} [\dots \int_{-3l/2}^{-l/2} T_0(x') \exp\left(-\frac{(x-x')^2}{4a^2t}\right) dx' + \\
 &+ \int_{-l/2}^{l/2} T_0(x') \exp\left(-\frac{(x-x')^2}{4a^2t}\right) dx' + \int_{l/2}^{3l/2} T_0(x') \exp\left(-\frac{(x-x')^2}{4a^2t}\right) dx' \dots]
 \end{aligned}$$

Taking into account the periodic condition $T(x + nL) = T(x)$, $n = \dots - 1, 0, 1, \dots$, and substitutions $x' = x'' + nL$, we can evaluate each of the above integrals within the interval $[-l/2, l/2]$:

$$\begin{aligned}
T(x, t) &= \frac{1}{2a\sqrt{\pi t}} \sum_{n=-N}^{n=N} \int_{-l/2}^{l/2} T_0(x'') \exp\left(-\frac{(x - x'' - nL)^2}{4a^2 t}\right) dx'' = \\
&= \frac{1}{2a\sqrt{\pi t}} \sum_{n=-N}^{n=N} \exp\left(-\frac{(nL)^2}{4a^2 t}\right) \int_{-L/2}^{L/2} T_0(x') \exp\left(-\frac{(x - x')^2 - 2nL(x - x')}{4a^2 t}\right) dx'.
\end{aligned}$$

B Workflow for calculating thermal conductivities using NEMD simulations

Algorithm 1

- 1: generate the simulation box and initialize velocities
 - 2: equilibrate at T_0 in the NVT ensemble using e.g. Nose-Hoover or CSVN thermostat
 - 3: divide the system into N_s slices along x-axis and switch off the thermostat
 - 4: **while** $t \leq t_{eq}$ **do** (*equilibration of the temperature perturbation*)
 - 5: **if** $t \bmod \Delta t = 0$ **then**
 - 6: compute current temperature in each slice
 - 7: rescale velocities in each slice in accordance to perturbation shape
 - 8: compute and subtract the total c.o.m. momentum
 - 9: **end if**
 - 10: **end while**
 - 11: $i = 1$
 - 12: **while** $i \leq M$ **do** (*generation of initial configurations*)
 - 13: keep the protocol the same as during equilibration
 - 14: **if** $t \bmod \tau = 0$ **then**
 - 15: save current configuration
 - 16: $i = i + 1$
 - 17: **end if**
 - 18: **end while**
 - 19: $j = 1$
 - 20: **while** $j \leq M$ **do** (*performing M relaxations*)
 - 21: run NVE simulation for t_r
 - 22: extract and save velocities to each slice at a given t
 - 23: $j = j + 1$
 - 24: **end while**
 - 25: compute the final $T(x, t)$ from stored velocities
 - 26: fit $T(x, t)$ with analytical solution and obtain $\kappa(t)$
 - 27: perform running average over $\kappa(t)$ and obtain the final κ .
-